Eleventh International Conference on Computational Fluid Dynamics (ICCFD11), Maui, HI, July 11-15, 2022

ICCFD11-2022-3202

Blowing Effects on the Material Response of an Orthotropic Charring Ablator

L.P. Askins* and A. Martin*
Corresponding author: Alexandre.Martin@uky.edu

*Mechanical and Aerospace Engineering, University of Kentucky, Lexington, KY 40506, USA.

Abstract: Blowing effects are one of the primary contributing factors to differences between 2D and 1D material response models. Analysis of TACOT, a surrogate material based on PICA, exposed to a set of arc-jet conditions gives some insight into the behavior of a charring ablator. Additionally, comparisons among TACOT, charred TACOT, and Fiberform - TACOT's non-phenolic preform - provide quantification and explanation for variations seen due to blowing phenomena. Graphite is used as the isotropic and non-pyrolyzing baseline to validate the predictions of the Kentucky Aerothermodynamics and Thermal-response System against experiment and 1D predictions using the Fully Implicit Ablation and Thermal Response Program. Comparisons between charring ablators and their non-pyrolyzing counterparts allow improved understanding of these effects.

Keywords: Thermal Protection Systems, Material Response, Arc-jet.

1 Introduction

Thermal protection systems (TPS) are used to protect objects that undergo atmospheric entry by preventing high temperatures from reaching the payload. Charring ablators are one of the more common types of TPS materials [1] due to their ability to mitigate the heat transferred to the material via pyrolysis gases [2]. Continued development of these materials requires improvements in experiments and computational fluid dynamics (CFD) and material response simulations. Understanding the blowing effects of pyrolysis gases as well as the orthotropic nature of these TPS materials is important, especially when characterizing the multidimensional nature of their behavior.

New orthotropic material models for charring ablators were recently implemented in the Kentucky Aerothermodynamics and Thermal-response System (KATS) in order to compare 2D models with experiments and 1D results using the Fully Implicit Ablation and Thermal Response Program (FIAT). In order to verify the proper behavior of these models, the case is first tested on TACOT, a material meant to phenomenologically replicate PICA [3], as well as its charred and preform versions. There is other established work developing this code for the mesh motion procedures as well as the transverse isotropic model implementation used in this work [4, 5], but the following work primarily focuses on understanding the effects of blowing on the material response of TACOT as compared to non-pyrolyzing materials. These three materials all exhibit similar orthotropic behavior, though properties among them vary slightly. TACOT can be analyzed to confirm the expected flow response. Additionally, a comparison among the three allows observations to be made on the 2D effects of blowing on the thermal response of the model. Graphite is first analyzed under the same boundary conditions in order to give a standard to compare to and validate the boundary conditions implemented in the model.

2 Test Cases

Comparisons can be made between Fiberform, TACOT, and charred TACOT to determine the effects of gas flow on material response when the materials are modeled under arc-jet conditions. In order to validate the model, the conditions are first run on a graphite model, and results are compared to experimental temperature measurements as well as a 1D model, FIAT [6]. Next, these same conditions are applied to the three materials. Parameters such as temperature, pressure, density, and velocity can be compared to show the resulting effects of pyrolysis gas blowing.

2.1 Boundary Conditions

The heating boundary conditions replicate those presented in previous work to represent the heating in the Aerodynamic Heating Facility (AHF), an arc-jet at NASA Ames [6]. The time-dependent heating conditions were inversely determined from a graphite test article's thermocouple measurements using FIAT-Opt, a tool previously used for reconstructing re-entry environments [7, 8, 9]. The maximum values were determined using CFD predictions of the arc-jet chamber and nozzle at the targeted facility conditions [10] and are documented in Table 1.

Table 1: AHF facility target conditions

Heat Flux [W/cm^2]	Target Pressure [kPa]	Enthalpy [MJ/kg]	Film Coefficient [kg/m^2-s]
241	7.25	20.1	0.1346

Each of these values is maintained for the duration of the test except for the applied heat flux, which follows an inversely determined time-dependent function shown in Eq. 1, where q_{max} is the value provided in Table. 1.

$$q_w = \frac{1}{q_{max}}(3.572 \times 10^{-1}x^5 - 6.769x^4 + 4.811 \times 10x^3 - 1.567 \times 10^2x^2 + 2.186 \times 10^2x + 1.315 \times 10^2). \quad (1)$$

The duration of each test case is 5 seconds for the graphite and 30 seconds for the TACOT models, each with .85 seconds at the beginning and end to linearly ramp the heat to and from zero. Each of the materials is run as a 4-inch iso-q, with pressure and heating profiles scaled according to the distance from the center-line of the test article as shown in Fig. 1.

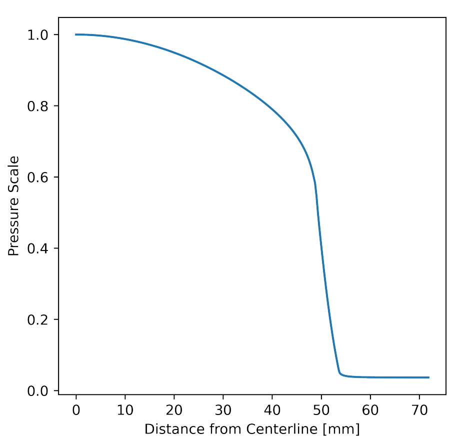

(a) Pressure

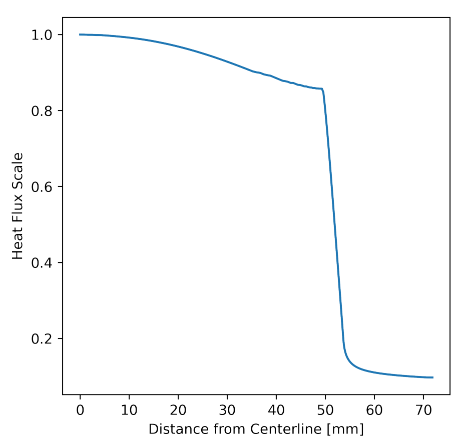

(b) Heat Flux

Figure 1: Scale for boundary conditions at given radial distance from center-line

2.2 Orthotropic Material Properties

Charring ablators often exhibit transverse isotropic rather than purely isotropic material properties [11]. The scheme for implementing these properties involves applying a rotational matrix to the property, typically permeability or thermal conductivity. This allows the in-plane value to be scaled up or down from the through-the-thickness value [5].

Values for this scale factor can be found using experimental measurements [12, 13], and are documented below in Table 2. Scales for TACOT's thermal conductivity are not available, but can be assumed using that of FiberForm [5].

Table 2: IP/TTT property scale factor

Material	Thermal Conductivity Scale	Permeability Scale
Graphite	1	1
Virgin TACOT	2.00	2.62
Char TACOT	1.74	1.41
Fiberform	1.74	2.01

2.3 Mesh

Two mesh independence studies were performed in order to quantify the variation of temperature in time and space when the number of cells is changed. A separate analysis is performed for the pyrolyzing case and the non-pyrolyzing cases because the former requires the addition of three momentum equations, whereas the latter group only requires the energy equation. For each study, the finest mesh is taken as the reference to which the other case/cases are compared. If the difference converges to a reasonably small number, the results are assumed to be accurate to a reasonable degree.

The non-pyrolyzing case only compares two meshes due to the relative simplicity of the case, with the coarser mesh having 3468 cells and the finer having 10143 cells. The pyrolyzing TACOT case is significantly more complex, so three additional cases with 8184 cells, 15163 cells, and 23848 cells are added. The coarsest of the meshes is pictured in Fig. 2, with each of the additional meshes retaining the same cell density.

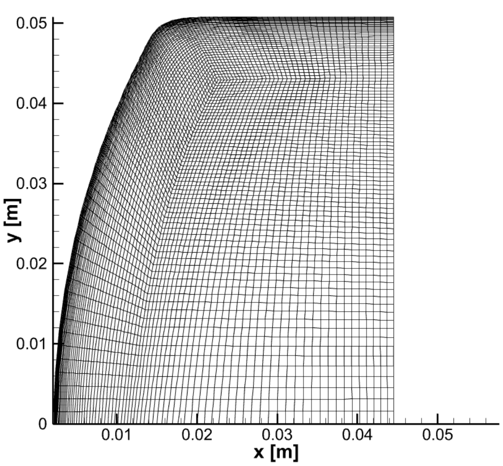

Figure 2: 3468 cell 4-inch iso-q mesh with $5 \times 10^{-}5$ meter wall refinement

Graphite is used as the sample case for the non-pyrolyzing set of boundary conditions. The variation in temperature would be slightly different for the TACOT cases due to a difference in material properties and duration, but the graphite model gives a reasonable indication of whether the two meshes provide a meaningful difference. In Fig. 3, the time-dependent temperature difference between the two meshes is shown at 2.5mm in depth, the location of the top thermocouple in the graphite test article run in the AHF test. The stagnation line temperature is also compared at its maximum, as the difference in temperature seems to increase over the period of heating.

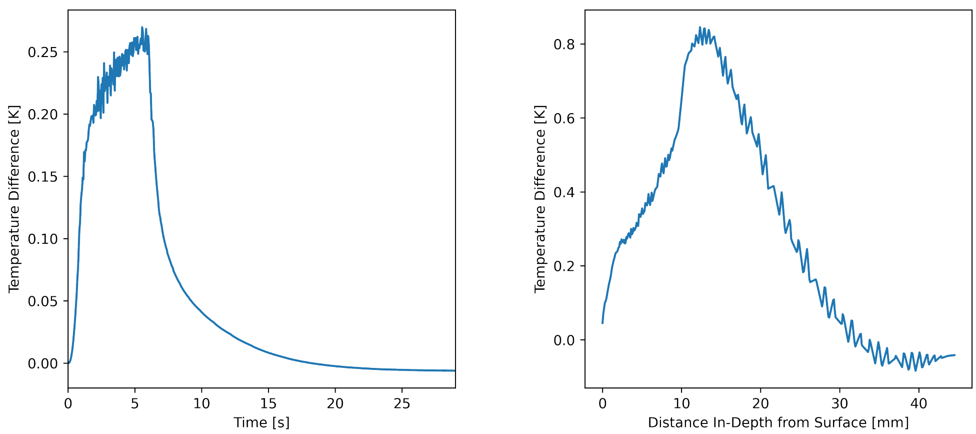

(a) 2.5mm in-depth

(b) Along stagnation line at 5.85 seconds

Figure 3: Graphite temperature difference between fine and coarse mesh

The maximum temperature differences are insignificant compared to the several hundred degrees experienced overall, so even the coarsest mesh is deemed sufficient to provide reasonably accurate results for the non-pyrolyzing materials. The only differences that may be seen in the non-pyrolyzing charred and preform TACOT cases would vary on material properties and duration, but the difference seen in graphite is so low that it is very unlikely a difference of more than a few degrees could be present. The TACOT cases also reach over 2000 K, so some increased variation would still be insignificant as compared to the huge temperatures.

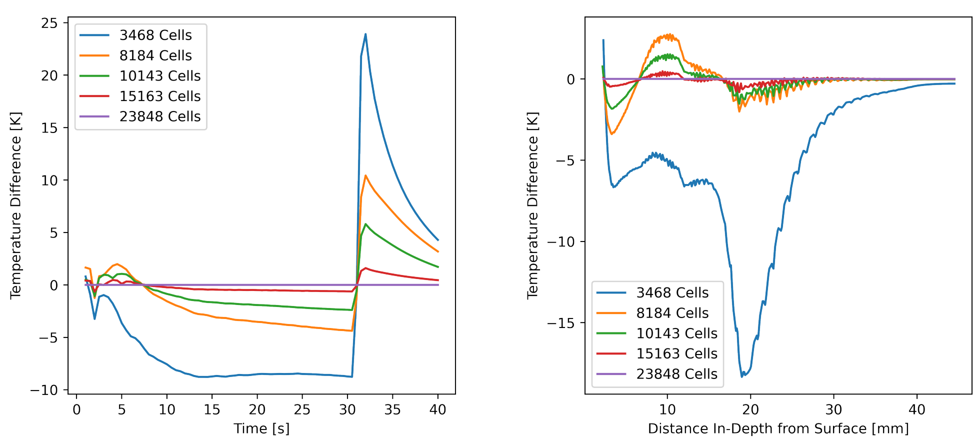

(a) 2.5mm in-depth

(b) Along stagnation line at 5.85 seconds

Figure 4: TACOT temperature difference between the coarsest mesh and each other mesh

The same analysis is performed for the five TACOT meshes, and the results are shown in Fig. 4. The pyrolyzing case shows a much greater dependence on the mesh size, but the largest amounts of temperature variation occur after the heating has ended. Additionally, the variation levels off to very low numbers after increasing to 15163 cells, so this mesh is deemed acceptable to provide reasonably accurate results for TACOT.

3 Results

3.1 Graphite

The previously discussed boundary conditions have been implemented in cases using 1D code FIAT [6], and the resulting temperatures, shown in Fig. 5, match thermocouple results to a high degree of accuracy. To validate the accuracy of these boundary conditions in TACOT cases, the same case is run in KATS in 2D. Because graphite is isotropic and non-pyrolyzing, the resulting center-line temperatures are expected to match the 1D results well.

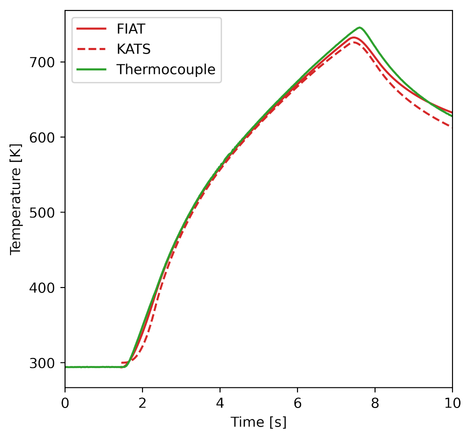

Figure 5: Temperature comparison between 1D and 2D at 2.5mm in depth from stagnation point

The resulting differences between the 1D and 2D temperatures at the top thermocouple location are very small, indicating that for isotropic non-pyrolyzing materials there is very little difference at the center-line between 1D and 2D models. This is to be expected, and provides a good baseline for comparing orthotropic materials with that in mind.

3.2 TACOT

Understanding the flow behavior within the TACOT material provides insight into its decomposition under high amount of heating. Characteristic material properties such as density, pressure, and velocity do not vary within the non-pyrolyzing cases with no momentum equations being solved, so the behavior of the flow within the TACOT is attributed primarily to the phenomenon of pyrolysis.

Figure 6 depicts the density, pressure, and velocity contours, which can be analyzed to understand the flow behavior. The density within TACOT behaves as expected, with a line of lower density developing on the surface to represent the charred and charring region. This char region propagates deeper into the material as time goes on, though areas along the surface disappear as the surface itself moves due to ablation. As the resin making up part of the material evaporates, the majority of the gas accumulates along the line of charring material. It then flows toward the regions where the density and pressure are lower. The very low pressure along the side creates a pressure differential that forces most of the gas width-wise and out the side, though some follows the slightly lower, but still significant, pressure differential into the material or toward the surface, depending on the location within the char region with respect to the surface. The streamline that moves width-wise along the material separates the flow moving toward and away from the surface due to blowing effects, and the location of this line aligns well with the charring region of the material at any given time. Additionally, the transverse isotropic nature of the permeability is having an effect here. The higher velocity in the in-plane directions as compared to the through-the-thickness direction is obvious in the analysis of the velocity's magnitude. This indicates that the orthotropic permeability is having an amplifying effect on the ability of the pyrolysis gases to move throughout the material.

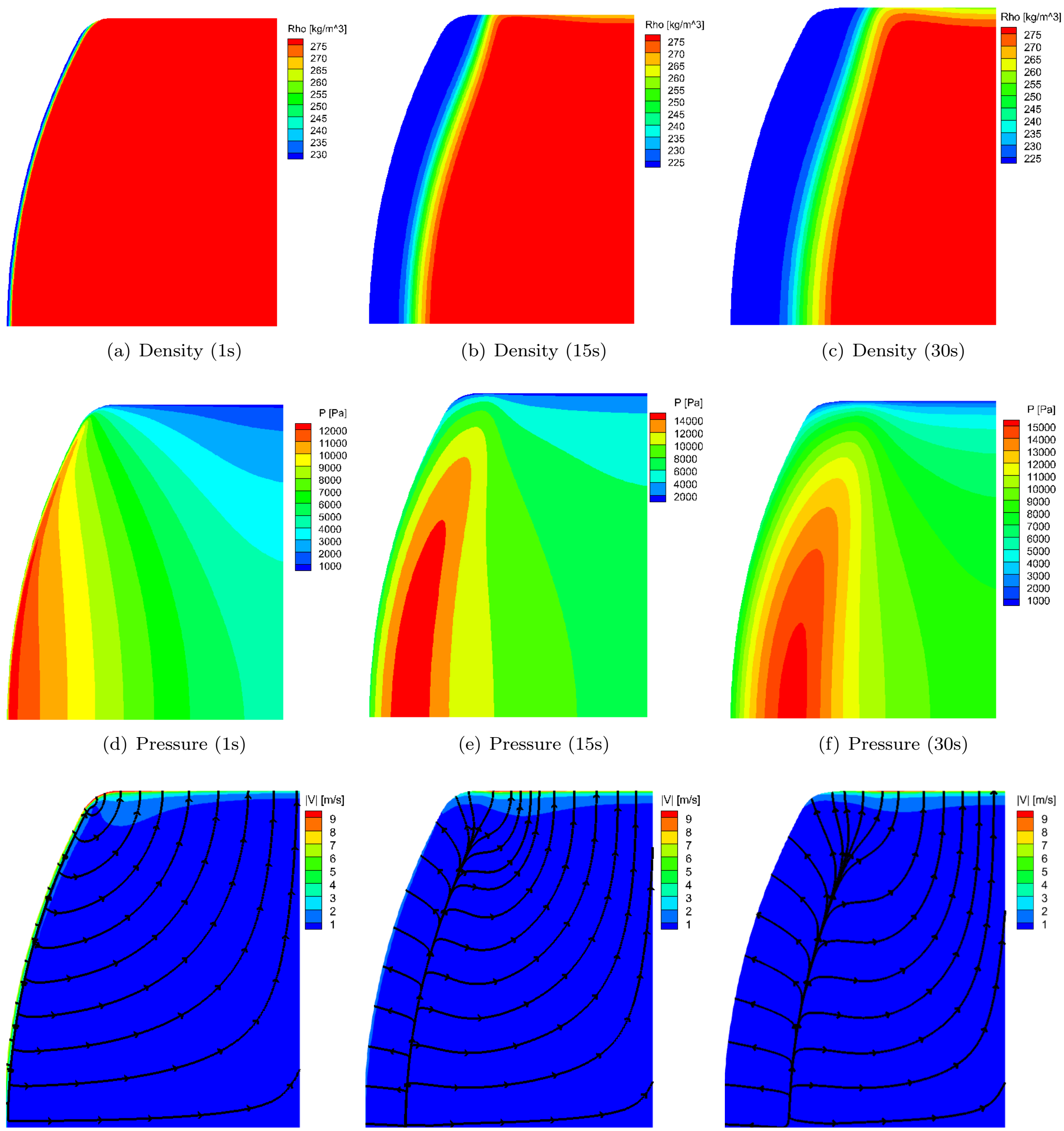

(a) Density (1s) (b) Density (15s) (c) Density (30s)

(d) Pressure (1s) (e) Pressure (15s) (f) Pressure (30s)

(g) Velocity Magnitude (1s) (h) Velocity Magnitude (15s) (i) Velocity Magnitude (30s)

Figure 6: TACOT density, pressure, and velocity contours and streamlines throughout duration

Though it shows little about the flow within the material, temperature is the most useful of the material response parameters to characterize as it is the property that TPS materials aim to minimize. Additionally, the ability to measure it inside the material during experiments makes it verifiable in ways that velocity and pressure are not. This makes the characterization of the previously described parameters of the flow useful as tools for understanding the impact of pyrolysis gas flow on temperature.

Temperature contours for TACOT are displayed in Fig. 7 at three points in the duration. While 2D effects are clear along the edge of the material, especially after a longer duration, the temperature gradients near the center-line appear to behave in a relatively 1D fashion, though the orthotropic material properties are having some effect. The lines of the contour roughly follow the shape of the surface, at least until they reach the region closest to the side wall. In this side region, interesting phenomena occur due to the blowing of gas at a high velocity out of the wall. A slight drop in temperature on the wall creates a visible bulge in low temperature regions toward the shoulder region, something often observed in the recession patterns of test articles exposed to high temperature flows. It reflects the same shape seen in the density contour, with a drop on the side reflecting additional side charring.

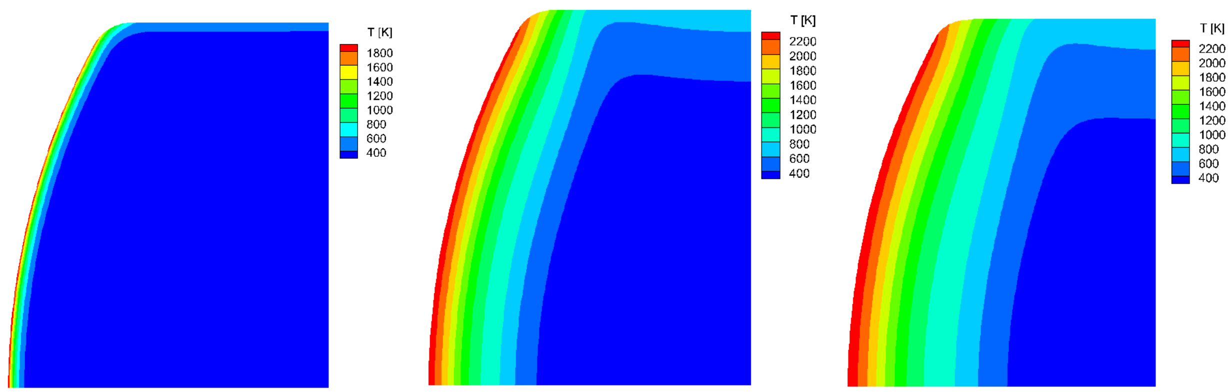

(a) Temperature (1s) (b) Temperature (15s) (c) Temperature (30s)

Figure 7: Temperature contours throughout duration

While the behavior of the side wall is interesting to note, the stagnation region and the center-line are the regions where thermocouples are placed and therefore are of primary interest for temperature analysis. A useful way to characterize 2D effects is to examine the temperature at the center-line at various times to discover any 2D effects that are difficult to discern in the contour.

Figure 8 depicts just this for TACOT, with the addition of Fiberform and TACOT's charred state for comparison. Some variations are going to occur among the three materials purely due to differences in material properties. For example, the densities of each is different, so the slope difference seen at 30 seconds among the three is not a surprise. However, the obvious effects of the blowing behaviour throughout the material is visible in the TACOT curve, especially longer into the duration. A decrease in the temperature gradient for a region in depth indicates a cooled region, increasing in size and depth over time. This region appears exactly at the location of the char region, which also increases in size and depth. This indicates the effects of blowing on temperature become stronger over time.

In addition, temperature gives a good indication of the impact of the transverse isotropic properties. Because the conductivity is higher in-plane than through-the-thickness, the 2D effects on temperature are intensified in the same ways as velocity. Heat propagates easier in-plane, likely helping to cause that lower temperature in TACOT at each point in time as compared to the char and Fiberform.

Surface temperature, shown in Fig. 9, is another useful parameter to understand the behavior of each of the three materials. The profiles of the temperature for each material at each time match the expected shape given by the heating profiles in Fig.1. TACOT appears to heat the slowest while Fiberform heats the fastest. TACOT has more prominent orthotropic effects, lower thermal conductivity, and the presence of cooling pyrolysis gases that all contribute to the lower surface temperatures compared to the other materials. Though it is more difficult to discern on the surface, the temperature bulge visible in the temperature contours is also present on the surface to some degree. Each of the materials nearly reaches a steady temperature by the end of the duration, with temperature gradients decreasing over time.

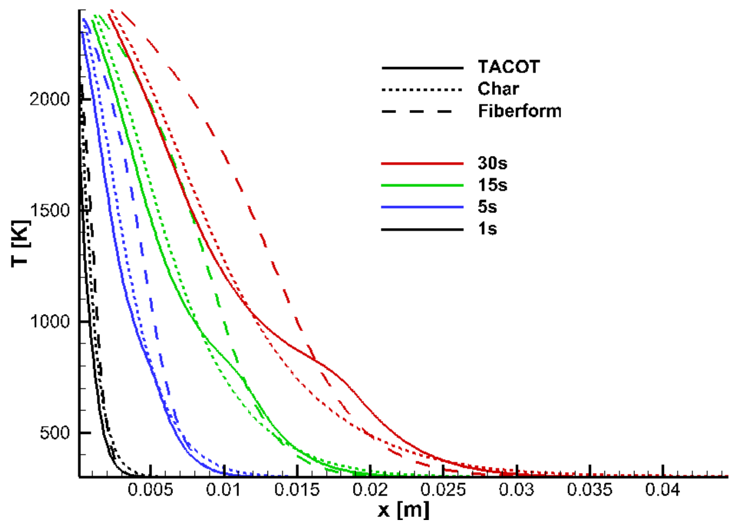

Figure 8: Center-line temperature throughout duration for TACOT, charred TACOT, and Fiberform

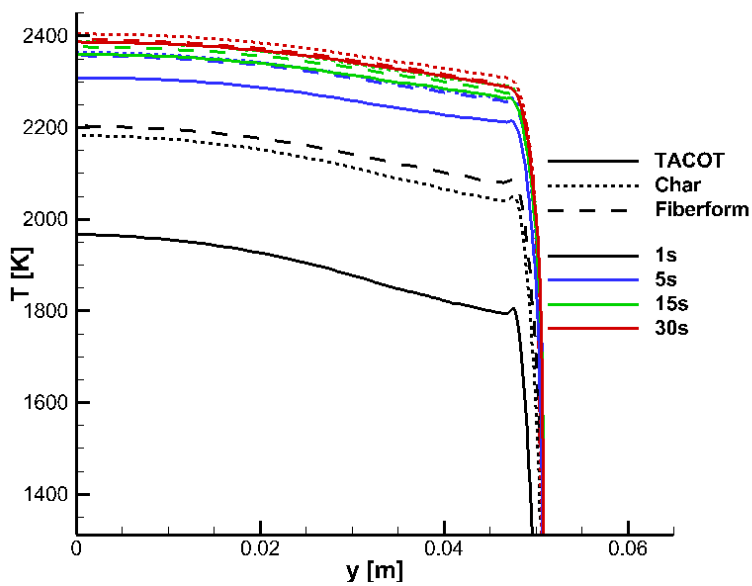

Figure 9: Surface temperature throughout duration for TACOT, charred TACOT, and Fiberform

4 Conclusions

Analysis of the 2D material response effects in purely isotropic and non-pyrolyzing materials provide insight into the behavior of TPS materials and pinpoint explanations for certain physical observations. An analysis of graphite allows a baseline for understanding an isotropic non-pyrolysing ablator's response to arc-jet test conditions. Comparisons to 1D and test measurements proved a distinct lack of 2D effects for this case and validated the code's accuracy.

The comparison of numerous materials, exposed to the same boundary conditions, provides additional insight to the effects of pyrolysis gas blowing on temperature. The most obvious effect is seen in the change in the temperature gradient along the char region in TACOT, which is not visible in either of the non-pyrolyzing materials. There is the additional observation of the temperature contour shape at the corner of the material. The lower temperature region reaching out toward the shoulder of the model is a direct result of blowing effects, and explains some observed phenomena from arc-jet tests.

Finally, the examination of velocity, pressure, and density provide explanation for these effects due to their presence only in the pyrolyzing case. The same bulging phenomena viewed on the temperature contours appear in the density contour, indicating side wall charring in addition to the front wall recession and charring. The pressure and velocity contours show that the pyrolysis gas builds up along the char region. While these gases blow in every direction, they primarily flow toward the side wall where the lowest pressure remains throughout the test. This results in the temperature phenomena observed previously. Overall, this work supports the presumption that 2D effects have a significant impact on flow properties and temperature in charring ablators.

5 Acknowledgments

This project was funded under NASA EPSCOR award 80NSSC21M0163. The authors would like to thank Ben Libben, Grant Palmer, and Joseph Williams for support on the arc-jet test analysis. The authors would also like to thank the University of Kentucky Center for Computational Sciences and Information Technology Services Research Computing for their support and use of the Lipscomb Compute Cluster and associated research computing resources.

References

[1] Deepak Bose, Todd White, Milad Mahzari, and Karl Edquist. Reconstruction of aerothermal environment and heat shield response of mars science laboratory. *Journal of Spacecraft and Rockets*, 51:1174–1184, 07 2014.

[2] Haoyue Weng and Alexandre Martin. Multidimensional modeling of pyrolysis gas transport inside charring ablative materials. *Journal of Thermophysics and Heat Transfer*, 28(4):583–597, 2014.

[3] Huy Tran, Christine Johnson, Daniel Rasky, Frank Hui, Ming-Ta Hsu, and Y. Chen. *Phenolic Impregnated Carbon Ablators (PICA) for Discovery class missions.*

[4] Aleksander L Zibitsker, Joel McQuaid, Christoph Brehm, and Alexandre Martin. Development and verification of a mesh deformation scheme for a three dimensional ablative material solver. In *AIAA SCITECH 2022 Forum*, page 1285, 2022.

[5] Haoyue Weng, Ümran Düzel, Rui Fu, and Alexandre Martin. Geometric effects on charring ablator: Modeling the full-scale stardust heat shield. *Journal of Spacecraft and Rockets*, 58(2):302–315, 2021.

[6] Page Askins, Alexandre Martin, Benjamin Libben, Grant Palmer, and Joseph Williams. Semi-empirical 1d material response modeling using inverse methods. In *AIAA AVIATION 2022 Forum*, 2022.

[7] Hannah Alpert, Milad Mahzari, David Saunders, Joshua Monk, and Todd R. White. Inverse estimation of mars 2020 entry aeroheating environments using medli2 flight data. In *AIAA SCITECH 2022 Forum*, 2022.

[8] Milad Mahzari, Robert D. Braun, Todd R. White, and Deepak Bose. Inverse estimation of the mars science laboratory entry aeroheating and heatshield response. *Journal of Spacecraft and Rockets*, 52(4):1203–1216, 2015.

[9] Milad Mahzari, Robert D. Braun, and Todd R. White. Reconstruction of mars pathfinder aeroheating and heat shield response using inverse methods. *Journal of Spacecraft and Rockets*, 50(6):1171–1182, 2013.

[10] Grant Palmer, Dinesh K. Prabhu, and Imelda Terrazas-Salinas. Arc jet facility test condition predictions using the adsi code. In *45th AIAA Thermophysics Conference*, 2015.

[11] Haoyue Weng and Alexandre Martin. Numerical investigation of thermal response using orthotropic charring ablative material. *Journal of Thermophysics and Heat Transfer*, 29(3):429–438, 2015.

[12] Jochen Marschall and Michael E. Cox. Gas permeability of lightweight ceramic ablators. *Journal of Thermophysics and Heat Transfer*, 13(3):382–384, 1999.

[13] Arnaud Borner, Francesco Panerai, and Nagi N. Mansour. High temperature permeability of fibrous materials using direct simulation monte carlo. *International Journal of Heat and Mass Transfer*, 106:1318–1326, 2017.